ARTICLE

https://doi.org/10.1590/2317-4889202120210048

BJGEO
Brazilian Journal of Geology

Deformation mechanisms, mineral chemistry and zircon U-Pb geochronological constraints in the south Patos shear zone: implications for the crustal evolution of the Borborema Province, NE Brazil

Carolina Peixoto de Souza[1], Luis Gustavo Ferreira Viegas[1]*, Lauro Cézar Montefalco de Lira Santos[2]

Abstract

The southern boundary of the Patos Shear Zone (PSZ) is characterized by mylonites resulting from the deformation of Paleoproterozoic basement gneisses, Neoproterozoic metavolcanic and metasedimentary rocks, granitic and granodioritic intrusions. Among the latter, the Santa Terezinha and Catingueira plutons show stretched shapes in agreement with the the shear zone's regional trend. Recrystallized quartz grains in these plutons accommodate deformation by dislocation creep. The host banded gneisses show similar deformation structures to the plutons. Quartz crystallographic fabrics mainly record the activity of basal and prism slip planes with local contribution of rhomb planes, whilst feldspar clasts show evidence of intracrystalline deformation in the larger porphyroclasts. These characteristics suggest that shearing occurred at lower-amphibolite facies conditions. U-Pb zircon data for the Santa Terezinha pluton yields an age of 625 ± 7 Ma, which, coupled with the pluton elongated shape and microstructure, suggests that its emplacement was pre-kinematic in relation to the Patos shear zone. Post-emplacement elongation of the granite body occurred along the strike-slip trend. Such structural and geochronological constraints highlight the close association between magma emplacement and shear zone deformation during distinct stages of the Brasiliano-Pan-African orogeny in the Borborema Province.

KEYWORDS: Patos shear zone; granitic magmatism; microstructures; geochronology; deformation mechanisms.

INTRODUCTION

Tectonic controls related to the emplacement and exhumation of granitic bodies along strike-slip zones have been largely studied for more than three decades (Hutton 1988, Paterson and Tobisch 1992, Vigneresse 1995, Vauchez *et al.* 1997, Rosenberg 2004). In addition to the record of final exhumation stages of large-scale structures, it is recognized that magma emplacement mechanisms play an important role in the chronology of deformational events in orogenic regions (*e.g.,* Brown and Solar 1998, Paterson *et al.* 1998, Schmidt and Paterson 2000, Weinberg *et al.* 2004).

Granitic plutons commonly occur parallel or slightly oblique to the main orientation of shear zones. When this relationship is established, they can be classified as pre-, syn- or post-kinematic (Hutton 1988, Vigneresse 1995, Vauchez *et al.* 1997). The timing of crystallization processes and subsequent shear zone deformation may be assessed by the pluton shape, its internal microstructures and fabrics, as well as its structural relationships with the host rocks (Hutton 1988, Brown and Solar 1999, Archanjo *et al.* 2002, Weinberg *et al.* 2004).

During the Brasiliano/Pan African orogeny (650-550 Ma) in Northeast Brazil, the tectono-thermal evolution of the Borborema Province (Fig. 1) was evidenced by a broad and diverse granitic magmatism mainly associated with NE-SW and E-W transcurrent shear zones (*e.g.,* Vauchez *et al.* 1995, Vauchez *et al.* 1997, Neves *et al.* 2000, Archanjo *et al.* 2008). Early U-Pb zircon data for this province's classic granites established three main magmatic events in *ca.* 650–625 Ma, 580–570 Ma, and 545–520 Ma (Sial and Ferreira 2016 and references therein). The integrated field, petrographic, and geochemical/isotopic investigation of the granitic plutons in distinct chronological scenarios share the common trait of their association with the major shear zones, providing reliable feedbacks between magmatism, deformation, and metamorphism (e.g., Vauchez *et al.* 1995, Santos and Medeiros 1999, Neves *et al.* 2000, Guimarães *et al.* 2004, Neves *et al.* 2006, Archanjo *et al.* 2008, Archanjo *et al.* 2013, Santos and Viegas 2021).

Bordering the southern limit of the Patos shear zone, an important structure present in the Borborema Province, there are medium to low- temperature mylonitic granites associated with high-temperature gneisses and metasedimentary rocks (Vauchez *et al.* 1995). Among them, the Catingueira and Santa Terezinha plutons have elliptical shapes that are concordant with the E-W mylonitic foliation of the shear zone, thus suggesting an intimate association of these granitoids with the strike-slip motion of the shear zone (Vauchez *et al.* 1997).

Despite previous data showing that the emplacement of both the Santa Terezinha and Catingueira plutons happened late in comparison

[1]Instituto de Geociências, Universidade de Brasília – Brasília (DF), Brazil. E-mails: carolinapdesouza@gmail.com, lgviegas@unb.br

[2]Departamento de Geologia, Universidade Federal de Pernambuco – Recife (PE), Brazil. E-mail: lauro.lsantos@ufpe.br

*Corresponding author.

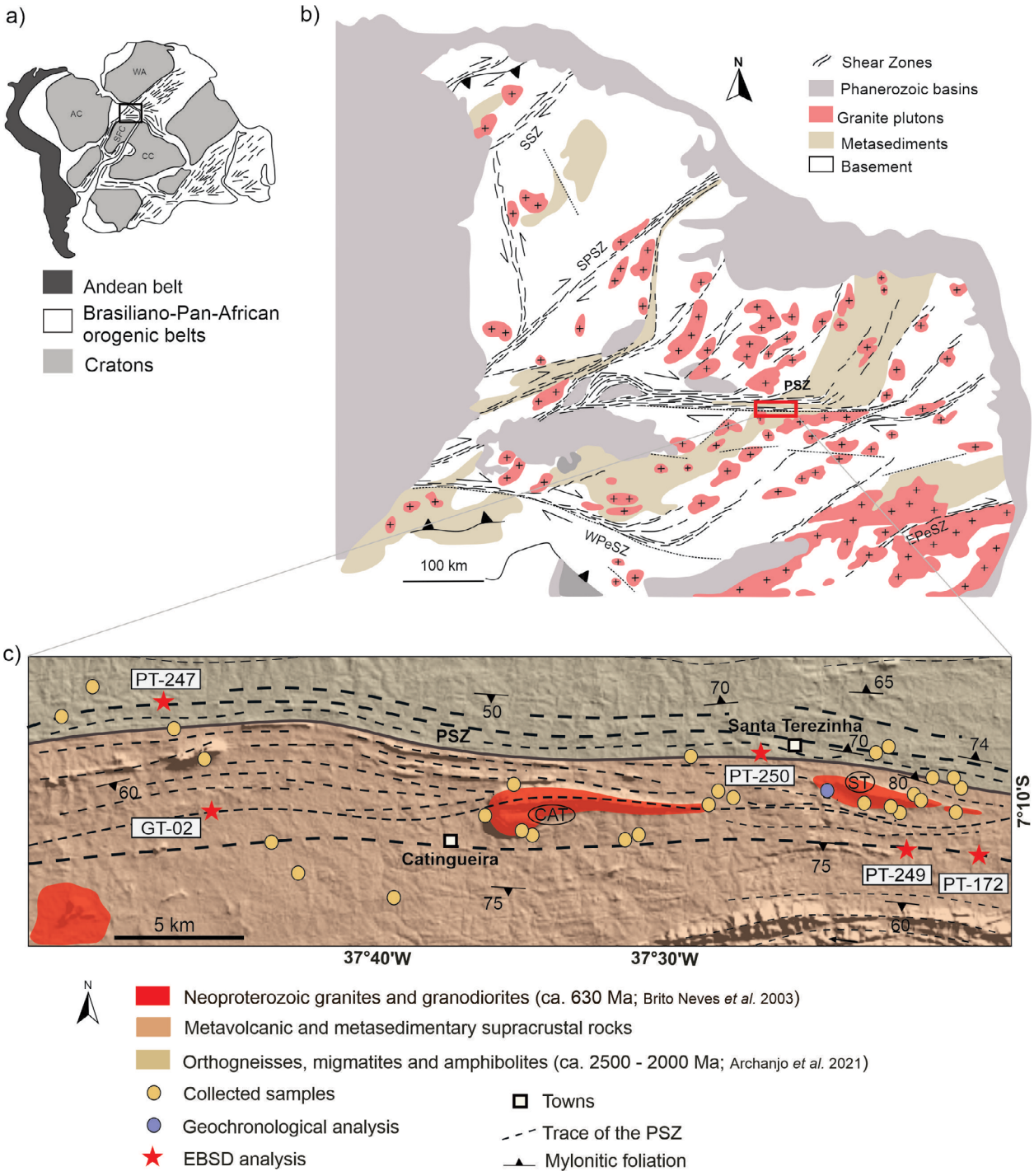

Figure 1. (A) Pre-drift reconstruction of South America-Africa exhibiting the Amazonian (AC), São Francisco (SFC), West African (WAC), and Congo (CC) Cratons, Brasiliano-Pan-African belts, and Andean Belt. The black square represents the Borborema Province; (B) Schematic map displaying the tectonic domains of the Borborema Province (northern, central, and southern) and the main shear zones: SSZ (Sobral Shear Zone); SPSZ (Senador Pompeu Shear Zone); PSZ (Patos Shear Zone); WPeSZ (West Pernambuco Shear Zone), and EPeSZ (East Pernambuco Shear Zone). The red square represents the study area; (C) Schematic geological map of the southern PSZ, displaying the Paleoproterozoic gneisses, migmatites and amphibolites of the basement, supracrustal rocks and Neoproterozoic granites and granodiorites (CAT-Catingueira pluton, ST-Santa Terezinha pluton). The locations of field mapping points (yellow dots), geochronological (blue dot), and EBSD samples (red stars) are shown. Regional units and lithological contacts compiled and modified from Brito Neves *et al.* (2003), Archanjo *et al.* (2008), Hollanda *et al.* (2010), and Archanjo *et al.* (2021).

to the deformation and kinematic framework of the Patos shear zone (Almeida 1967, Sial 1986, Vauchez *et al.* 1997, Brito Neves *et al.* 2003), detailed geochronological and structural constraints on pluton emplacement mechanisms and the relationships between these intrusions and the medium to low-temperature metamorphism of the southern boundary of the Patos shear zone are still lacking.

This contribution presents the results of integrated field structural mapping, microstructural and crystallographic fabric analyses of the Catingueira and Santa Terezinha plutons and their host rocks in an attempt to investigate the deformation mechanisms that were active during the pluton emplacement and coeval shear deformation in the south Patos shear zone. In addition, we present a possible pluton emplacement age within the shear zone based on U-Pb zircon dating of the Santa Terezinha granite. Our results shed light into the chronological relationships between magmatism and deformation in

the southern sector of the Patos shear zone and highlight the importance of this structure in the frame of the Borborema Province's tectonic evolution.

GEOLOGICAL SETTING

The Borborema Province (NE Brazil, Figs. 1A and 1B) is a wide orogenic system formed by convergent episodes between the Amazonian, São Francisco, West African, and Congo cratons during the assembly of the West Gondwana (Almeida *et al*. 1981, Brito Neves *et al*. 2000, Caxito *et al*. 2020, Santos *et al*. 2021). It represents a major record of the Brasiliano orogeny (ca. 650–550 Ma), in which progressive deformation and magmatism culminated in the record of several granitoid plutons emplaced along a complex continental scale shear zone system (Vauchez *et al*. 1995, Brito Neves *et al*. 2003, Weinberg *et al*. 2004).

The structures form a conjugate system that extends for more than 200.000 km^2 and can be correlated with shear zones at the west African border (e.g. Brito Neves *et al*. 2000; Fig. 1A). E-W, dextral strike-slip ductile faults such as the Patos and Pernambuco shear zones are major markers of the Brasiliano orogeny and were proxies to define the the Borborema Province's Northern, Central and Southern domains(Fig. 1B; Van Schmus *et al.* 1995, Van Schmus *et al.* 2008).

The Patos shear zone (Figs. 1B and 1C) extends for approximately 600 km in the E-W direction and divides the Northern and Central tectonic domains (Fig. 1B). This structure is mainly characterized as a dextral strike-slip shear zone that comprises high temperature, amphibolite-facies mylonites in the northern, central and western portions, which were variably affected by partial melting episodes (Corsini *et al*. 1991). The best estimated age for the metamorphic peak is around 566 ± 6 Ma, obtained through the U-Pb SHRIMP-zircon dating in synkinematic leucosomes (Viegas *et al*. 2014, Archanjo *et al*. 2021).

The southern boundary of the shear zone is marked by the occurrence of mylonitic, banded gneisses and granitoid plutons, such as the Catingueira and Santa Terezinha granitoids, which occur parallel and/or slightly oblique to the E-W direction of the structure (Fig. 1C). These granites have elongated shapes, at approximately 1 km wide and 10 km long, cross-cutting the metasedimentary and metavolcanic rocks of the Cachoeirinha-Salgueiro belt (Vauchez *et al*. 1997, Brito Neves *et al*. 2000, Van Schmus *et al*. 2011). Solid-state deformation is observed in these granitoids, leading several authors to suggest that the intrusions were affected by the Patos shear zone (*e.g.,* Vauchez *et al*. 1997).

The selected area for this study is situated in the southern boundary of the central sector of the Patos Shear Zone (Fig. 1C), which is composed of Paleoproterozoic metagranitic to gneissic basement rocks, Neoproterozoic metavolcanosedimentary rocks and granites (Corsini *et al*. 1991, Archanjo *et al*. 2008, Viegas *et al*. 2014). Brito Neves *et al*. (2003) suggested a crystallization age of 573 ± 45 Ma, based on zircon U/Pb dating of a homogeneous leucocratic syenogranite, located in a quarry close to the town of Catingueira.

METHODS

Microstructures and EBSD analysis

A total of twenty-three oriented and polished thin sections were cut in the XZ plane of the structural reference frame, perpendicular to the foliation (Z) and parallel to the lineation (X). Deformation microstructures and petrographic aspects were studied via polarized light and electron microscopy at the Electron Microscopy Laboratory of the University of Brasília, Brazil. The crystallographic fabrics of the recrystallized quartz grains were studied via electron backscatter diffraction (EBSD) analysis at *Géosciences Montpellier, Université Montpellier 2* (France). Sample locations can be seen in Fig. 1C.

In order to ensure a well-polished surface for the samples, a chemo-mechanical polishing using colloidal silica was applied for ~2-3 hours. To avoid the effects of electron charging and subsequent low-image quality during the analyses, the polished thin sections were carbon-coated when the SEM was in high-vacuum mode and left uncoated if the SEM operated under low-vacuum conditions. EBSD analysis of characteristic areas of the deformed/recrystallized microstructure was performed with a JEOL JSM 5600 scanning electron microscope (SEM) equipped with an Oxford Instruments/HKL Nordlys EBSD detector. Data was obtained with the Channel5 software (Oxford Instruments), at analytical conditions of 75º sample tilt, working distance of 25 mm and 17 kV accelerating voltage. Step sizes ranged from 0.5 to 4 μm depending on the microstructural heterogeneity.

The treatment of EBSD data was performed with the MTEX version 5.0.3 toolbox for MATLAB (Hielscher and Schaeben 2008), which was used to generate pole figures, misorientation axes, and misorientation angle distributions. In the latter, pseudosymmetry effects on quartz grains, mainly due to dauphiné twinning, were corrected before plotting the crystallographic orientations in orientation diagrams. Pole figures were plotted as contoured diagrams in which the average orientation of the grains is represented as one point per grain. The contouring of the quartz crystallographic axes orientations was constructed based on multiples of uniform distribution (M.U.D.).

Mineral chemistry

The chemical composition of feldspars (porphyroclasts and recrystallized grains) in the granitoids was measured using a Jeol JXA 8230 Electron Probe Micro Analyzer at the Electron Microprobe Laboratory, Universidade de Brasília. The analysis was obtained with an accelerating voltage of 15-20 kV, current of 5 nA, and beam diameter of 1 μm for K-feldspar and 5 μm for plagioclase.

Zircon U-Pb geochronology

A sample of the Santa Terezinha pluton (PUR-02D; location in Fig. 1C) was selected for zircon U-Pb age dating at the Geochronology Laboratory, Universidade de Brasilia. The sample was initially crushed and sieved, then the heavy minerals were separated using conventional gravimetric and magnetic methods. Zircon grains were then handpicked using a binocular microscope, mounted on the epoxy resin (0.5 cm), and polished (1 μm) for Laser Ablation Multi Collector Inductively

Coupled Plasma Mass Spectrometry (LA-MC-ICP-MS) isotope ratio acquisition.

Backscatter images of the analyzed zircon crystals were acquired with analytical conditions of 10 nA beam current, 20kV accelerating voltage, and 13.8 mm working distance. The laser ablation system used was ESI/New Wave Research, UP-213, Nd: YAG, with low volume cell (ca. 4 cm^3). The laser wavelength was 213 nm, with 3ns pulse width, fluence from 3.0 to 3.5 J cm^{-2}, repetition rate 10 Hz, spot size 25 µm, and carrier gas of 100% He, Ar make-up gas combined using a Y-piece along the sample transport line close to the torch.

The duration of pre-ablation laser warm-up was about 10 s, the ablation duration was about 40 s. The wash-out delay was about 20 s, whilst the used ablation pit depth was approximately ~10 µm, and the cell carrier gas flow 0.40 l min-1 He. Isotopic analyses were performed on a Thermo-Fischer, Neptune, MC-ICP-MS, ablation aerosol, 1050 W, 0.997 l min-1 sample gas flow, mixed Faraday cups, and multiple ion counting (MIC) array. The masses measured were Faraday ^{232}Th, ^{238}U, and ^{206}Pb, and MIC ^{202}Hg, ^{204}Pb, ^{207}Pb, and ^{208}Pb, with a total integration time per output data point of 1.049 s. Normalization was performed to the GJ1 zircon standard (Jackson *et al.* 2004, Horstwood *et al.* 2016) as the primary reference material and the 91500 (Wiedenbeck *et al.* 1995) was used as a secondary validation.

The data processing package used was Iolite v. 4. 0 (Paton *et al.* 2011) & VizualAge (Petrus and Kamber 2012), using exponential plus linear modeling for LIEF correction. The quality control was about 91,500 – Conc age = 1,063 ± 3 (2s, MSWDc+e = 0.27, n = 16) and the systematic uncertainty for propagation was 1% (2s). The age calculations were performed using in-house developed Excel spreadsheets and all U–Pb plots were created using the Isoplot software (Ludwig 1993).

RESULTS

Field and petrographic observations

In the studied area, most rocks commonly exhibit an E-W to WNW-ESE-trending mylonitic foliation evidenced by millimeter to centimeter-scale elongated quartz ribbons and stretched K-feldspar porphyroclasts.

The basement banded gneisses (Fig. 2A) are composed by felsic and mafic rocks. The felsic bands are characterized

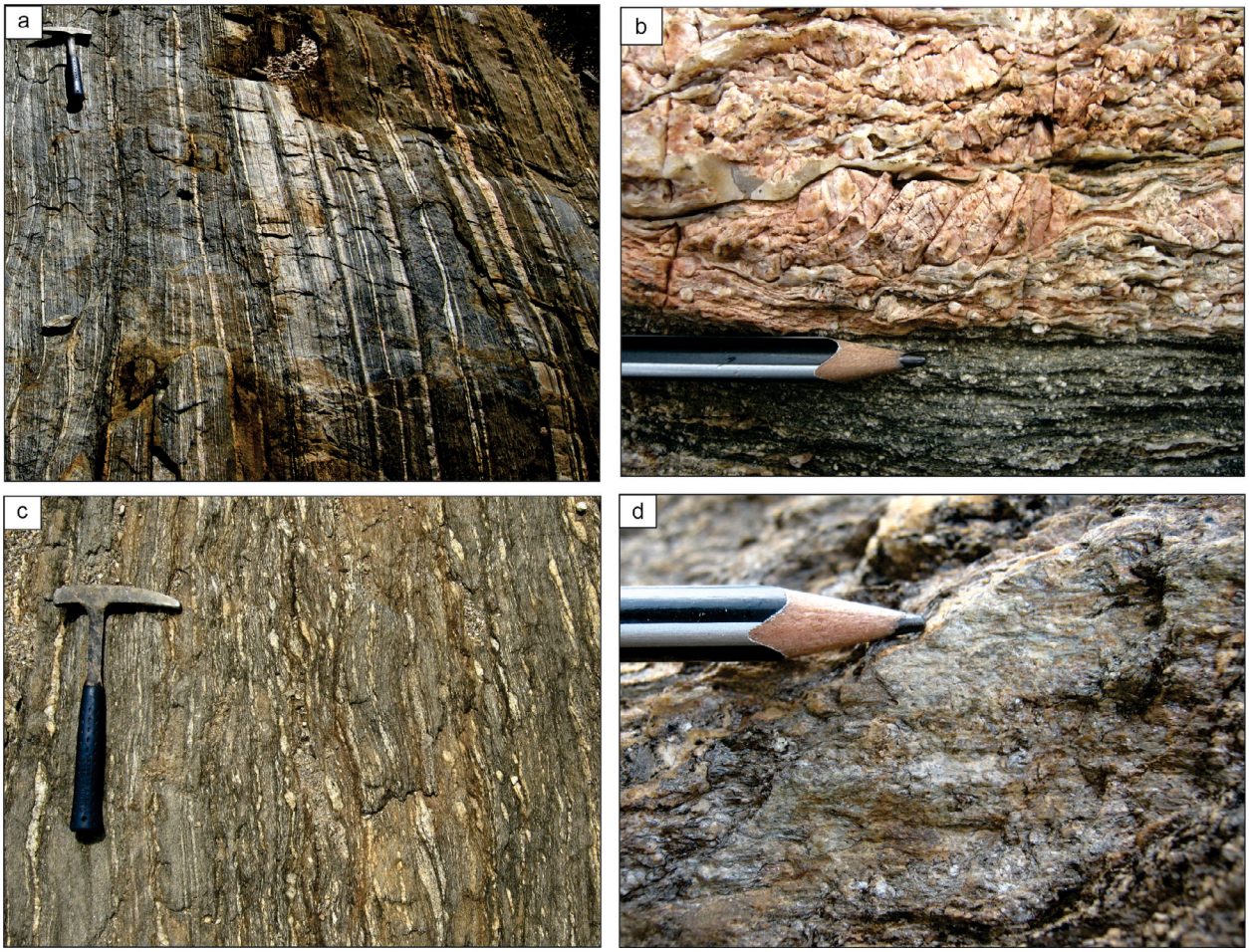

Figure 2. Field aspects of the basement rocks and metasedimentary sequences from the southern boundary of the Patos shear zone. (A) Banded gneiss showing fine to coarse-grained mafic and felsic bands, both parallel to the E-W mylonitic foliation of the Patos shear zone. (B) Contact between the mafic and felsic bands. The mafic band shows millimetric biotite crystals aligned to the mylonitic foliation, in addition to elliptical quartz grains and elongated feldspars. The felsic band presents centimeter-scale porphyroclasts of K-feldspar that are elongated and fractured. A quartz band parallel to the mylonitic foliation is observed close to the K-feldspar porphyroclast. (C) Medium- to coarse-grained metasedimentary rock with elonganted and stretched feldspar porphyroclasts immersed in a fine-grained, dark matrix; (D) Muscovite-rich, fine-grained metasedimentary rock with ultramylonitic texture. The mylonitic foliation is marked by elongated muscovite and biotite that are aligned with subordinate, stretched K-feldspar porphyroclasts.

of K-feldspar (20-30%), plagioclase (15-25%), quartz (15-20%), and biotite (5-10%). They comprise centimeter-scale quartz crystals and elongated porphyroclasts of K-feldspar that are fractured and have *augen*-shaped morphologies (Fig. 2B). The mafic bands show elongated biotite crystals (25-40)%), in addition to quartz grains (20-35%), and stretched feldspars (10-15%), both with millimeter sizes (Fig. 2B). The contact between the bands is abrupt and locally transected by oblique fractures. Quartz ribbons are parallel to the mylonitic foliation (Fig. 2B).

Muscovite-bearing metasedimentary rocks occur interspersed with the banded gneisses. They present a light grey to brown color and have a silky textural aspect. Quartz, biotite, muscovite and K-feldspar are the main mineral phases. In some portions, a porphyroclastic texture is observed, defined by elongated and fractured K-feldspar porphyroclasts that are immersed in a polymineralic, fine-grained matrix (Fig. 2C). A gradual transition from a medium-grained, mylonitic fabric to a fine-grained fabric that resembles an ultramylonitic texture (Figs. 2C and 2D) is observed via: increase in the matrix percentage and distribution in comparison to coarse grains, progressively decreasing in grain size coupled with gradual absence of porphyroclasts, preferred orientation of biotite and muscovite lamellae, and stretching of the K-feldspar clasts.

The Santa Terezinha pluton is characterized by a 5 km elongated body that is concordant with the WNW-ESE trend of the Patos shear zone (Fig. 1C). It is composed of quartz (20-30%), K-feldspar (20-25%), plagioclase (15-20%), biotite (7-10%), and muscovite (2-5%). The granite color ranges from light to medium grey, and a mylonitic, porphyroclastic texture is widespread (Figs. 3A and 3B). The centimetric K-feldspar porphyroclasts are elongated, locally *augen*-shaped and wrapped in millimeter-scale stretched biotite crystals (Fig. 3B).

The Catingueira pluton is an E-W, elongated *en-cornue* intrusion of ~12 km in length (Fig. 1C). The main mineral assemblage comprises K-feldspar (30-35%), plagioclase (20-30%), quartz (15-20%), biotite (10-15%), and amphibole (5-10%). The granite has a light grey, equigranular texture and an incipient foliation that is evidenced by the preferred orientation of millimeter-scale biotite lamellae (Fig. 3C).

Microstructures

Basement banded gneisses

The host banded gneisses are characterized by porphyroclasts of K-feldspar and plagioclase (500 μm – 3, 5 mm) that are wrapped in quartz ribbons (ribbon size - 50 to 200 μm),

Figure 3. Field aspects of the Santa Terezinha and Catingueira plutons. The coin used for scale is 23mm in diameter.: (A and B) Santa Terezinha granite showing a porphyroclastic texture marked by elongated K-feldspar porphyroclasts wrapped in quartz aggregates forming ribbons. Biotite crystals parallel to quartz grains evidence the mylonitic foliation. K-feldspar porphyroclasts can develop *augen* morphologies; (C and D) Catingueira pluton showing a light grey color, fine-grained equigranular texture, and an incipient foliation that is evidenced by the preferred orientation of millimetric biotite crystals.

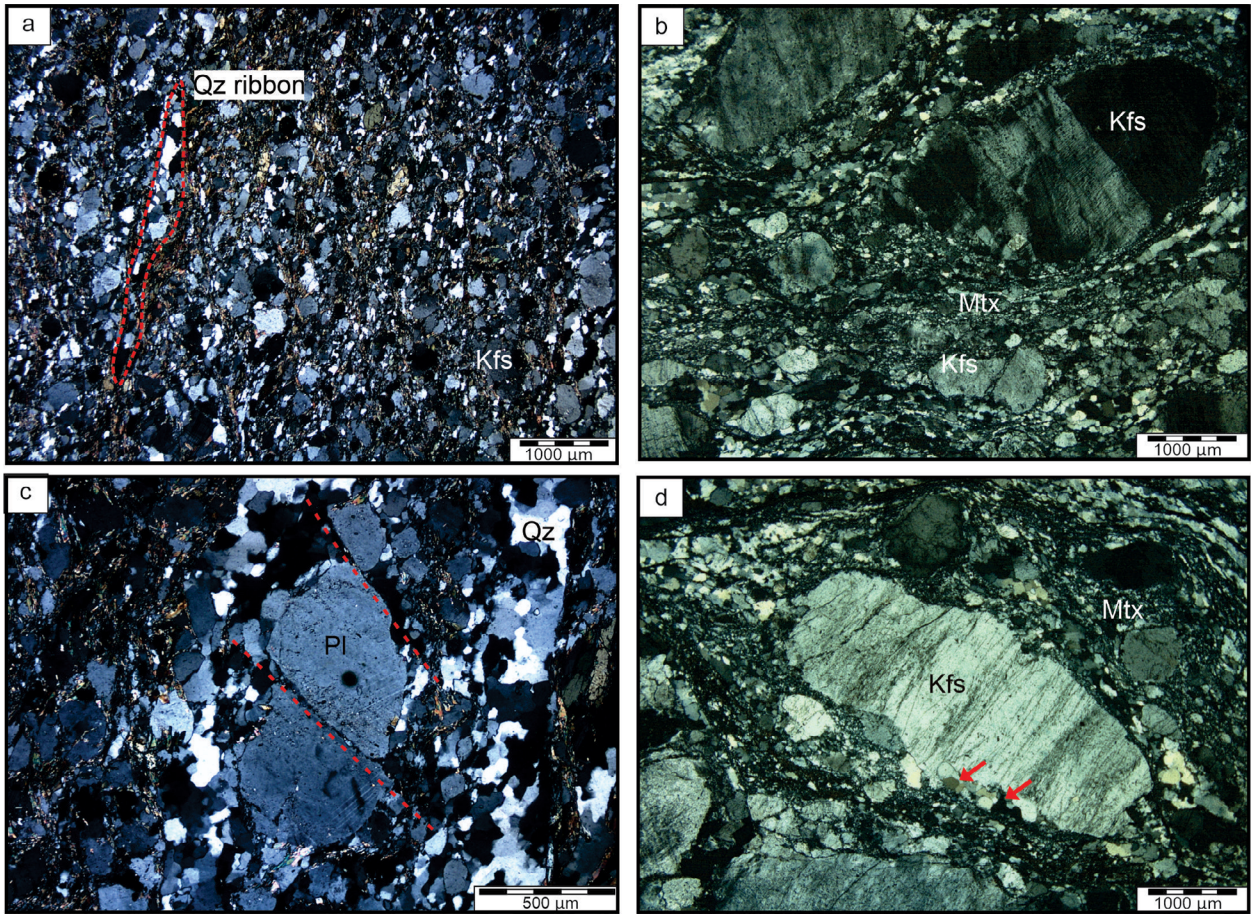

Figure 4. Microstructures in the banded gneisses of the southern Patos shear zone (Qz: quartz, Kfs: K-feldspar, Pl: plagioclase, Bt: biotite, Whitney and Evans 2010; Mtx: matrix) (A and B) Overview of typical mylonitic granite with porphyroclasts of K-feldspar and plagioclase wrapped in quartz ribbons and fine-grained recrystallized K-feldspar, plagioclase, quartz and biotite. The mylonitic foliation is defined by the preferred orientation of quartz ribbons, elongated feldspar clasts, and oriented biotite; (C and D) Sub-elliptical K-feldspar and plagioclase porphyroclasts embedded in the fine-grained recrystallized matrix and showing undulose extinction. A sinistral shear sense defined by asymmetric displacement along oblique microfractures is locally observed in plagioclase clasts [C]; Recrystallized grains rimming K-feldspar clast (red arrows) are strain-free and have lobate boundaries [D].

and a fine-grained recrystallized matrix (30–50 µm) mainly composed of quartz + feldspar + biotite (Fig. 4A).

The porphyroclasts of K-feldspar and plagioclase display sub-elliptical to rounded shapes and lobate boundaries (Figs. 4B, 4C and 4D). Some clasts show recrystallized, strain-free grains at their boundaries; these grains have around 150 µm, anhedral shape, and lobate boundaries (Fig. 4D). The clasts exhibit perthitic texture, undulose extinction and deformation twins (Figs. 4B, 4C and 4D). Microfractures commonly crosscut the clasts forming angular fragments (± 800 µm) and record offsets of up to 50 µm (Fig. 4C). Locally, the relationship of the microfractures with the wrapping foliation defined by the quartz aggregates may suggest sinistral shear sense at the scale of the porphyroclast (Fig. 4C).

Quartz crystals occur as polycrystalline ribbons with aspect ratios varying from 1:10 to 1:20 (Fig. 4A). The grains range from 50 to 200 µm with lobate boundaries and undulose extinction (Figs. 4A and 4C). The contact of quartz ribbons with the surrounding grains is mainly straight and occur parallel to the WNW-ESE-trending mylonitic foliation (Figs. 4A, 4B and 4D).

The recrystallized matrix comprises quartz (± 30 µm), feldspar (± 30 µm), and biotite (± 50 µm; Figs. 4A-4D), where the feldspar displays rounded shapes and lobate boundaries. Quartz crystals occur in rounded to polygonal shapes and lobate to straight boundaries. The biotite grains have elongated shapes and are subparallel to the mylonitic foliation (Figs. 4A and 4C).

Santa Terezinha Pluton

This pluton is characterized by a mylonitic fabric consisting of porphyroclasts of feldspar wrapped in quartz ribbons. These two microstructural domains, which comprise the bulk of the texture of the rock, are embedded in a fine-grained, recrystallized polyphase mixture of quartz, feldspar and biotite (Figs. 5A and 5B).

The porphyroclasts are mainly K-feldspar and plagioclase with grain sizes ranging from 700 µm to 2.5 mm. The clasts are sub-elliptical and have aspect ratios around 1:3 (Figs. 5B, 5C and 5D). They display irregular, straight subgrain boundaries as well as a weakly developed undulose extinction. Perthites and mechanical twins are observed in some of the K-feldspar and plagioclase clasts. Intragranular and transgranular microfractures show an average thickness of 30 µm (Figs. 5B, 5C and 5D).

The intragranular microfractures are straight and may be filled with fragments from the host clast and fine grains of the matrix (± 15 µm; Figs. 5C and 5D). They display kinematic offsets up to 100 µm and may result in sets of fractures that crosscut most of the coarse feldspar clasts (Fig. 5B). Some clasts display recrystallized

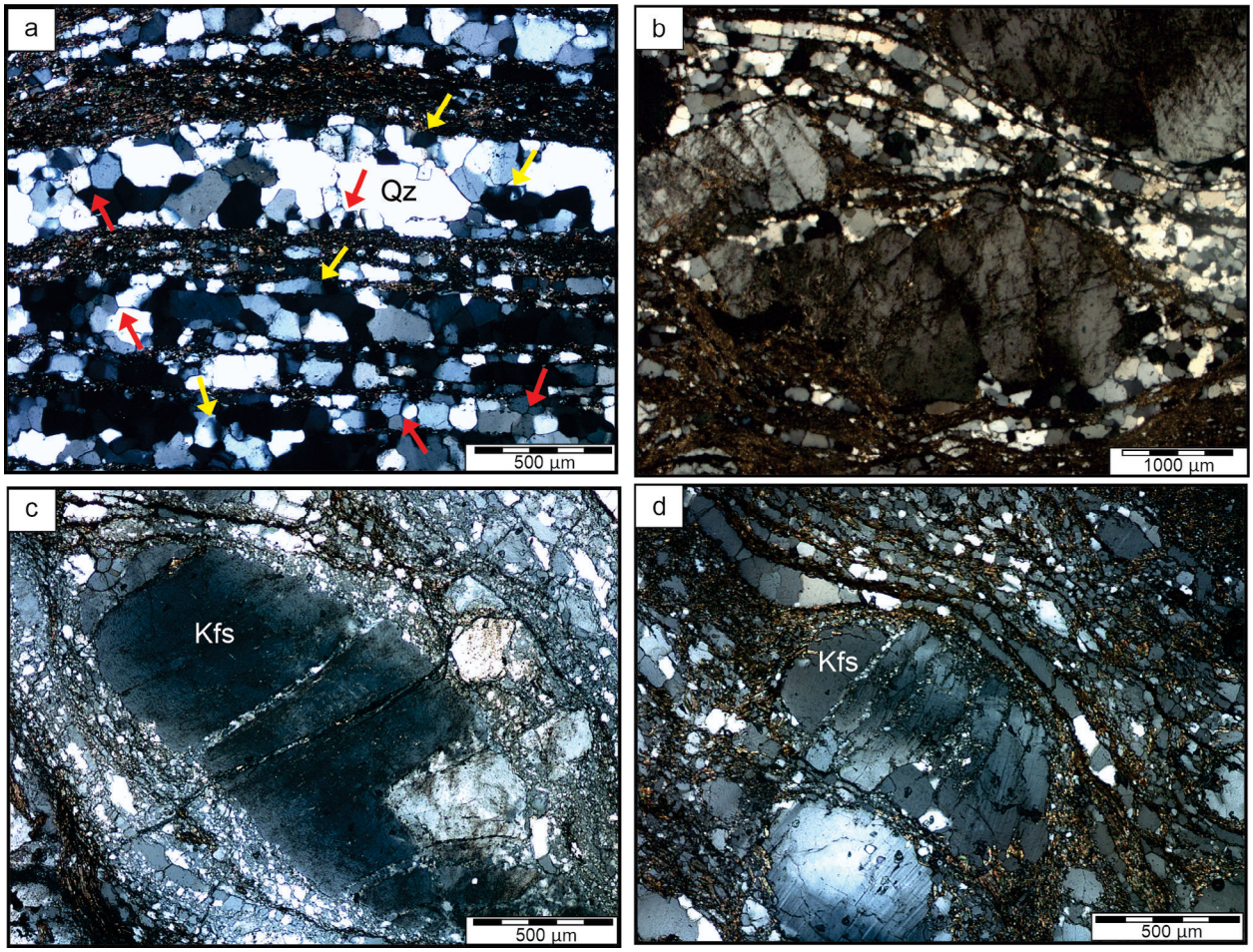

Figure 5. Microstructures of the Santa Teresinha pluton (Pl: plagioclase; Kfs: K-feldspar; Qz: quartz; Whitney and Evans 2010). (A) Foliation-parallel quartz ribbons with undulose extinction and straight boundaries that define triple junctions (red arrows). Yellow arrows indicate subgrains; (B) Microfracture sets crosscutting plagioclase porphyroclasts; quartz ribbons (upper right) are in discrete contact with the clasts; (C and D) Sub-elliptical K-feldspar porphyroclasts displaying microfractures filled by the fine-grained matrix and surrounded by quartz ribbons.

asymmetric tails composed of feldspar grains (± 10 µm), quartz crystals (± 25 µm) and fine grains of the polyphase mixture (quartz + feldspars + biotite; ± 10 µm; Fig. 5C).

Quartz occurs mainly as polycrystalline ribbons with aspect ratios varying from 50:1 to 10:1 with average grain sizes of 150 µm (Figs. 5A and 5D). The crystals have polygonal to irregular shapes that define both rectangular and straight grain boundaries typical of triple junctions (Fig. 5A). Typical substructures are undulose extinction and subgrain boundaries (Fig. 5A). The subgrains have ± 50 µm and straight to curved boundaries.

The recrystallized matrix is composed of fine-grained plagioclase (± 20 µm), K-feldspar (± 20 µm), quartz (± 15 µm), and biotite (± 10 µm; Figs. 5C and 5D). Feldspar grains display slightly rounded shapes, curved boundaries and weak undulose extinction. The quartz has irregular shapes and curved to straight boundaries, whilst the biotite crystals are elongated and parallel to the mylonitic foliation.

Catingueira Pluton

The microstructure of the Catingueira monzogranite comprises feldspar porphyroclasts (500 µm – 2 mm) that are wrapped in quartz aggregates (± 270 µm in length) and immersed in a fine-grained, quartz-feldspathic matrix (± 50 µm; Figs. 6A, 6B and 6C). Feldspar porphyroclasts are typically sub-elliptical and have straight boundaries (Figs. 6A and 6B). Microstructures are characterized by weak undulose extinction and deformation twins (Figs. 6A and 6B). Discontinuous intragranular microfractures are observed in the clasts and some are filled by elongated quartz crystals (± 50 µm; Fig. 6A).

Quartz occurs as coarse-grained polycrystalline aggregates with an average grain size of 200 µm. These grains have polygonal to irregular shapes and straight boundaries that define 120º - triple junctions (Figs. 6B, 6C and 6D). Locally, subgrain boundaries occur with subgrain sizes around 50 µm and curved to straight boundaries (Figs. 6C and 6D). Amphibole crystals are partially altered to biotite and range from 500 µm to 1 mm (Figs. 6B and 6D). They also have an elongated shape, straight to irregular boundaries and are parallel to the foliation (Figs. 6B and 6D).

The fine-grained matrix comprises mainly recrystallized quartz and feldspar grains with an average grain size of 30 µm (Figs. 6A and 6B). Both show curved grain boundaries, with quartz grains locally displaying straight boundaries.

EBSD analysis of quartz CPO in the host banded gneisses

Quartz crystallographic fabrics (Figs. 7A-7E) in the banded gneisses are marked by two main patterns: small maxima of the c-axis at the periphery of the diagram, close to Z (PT 172, Fig. 7A)

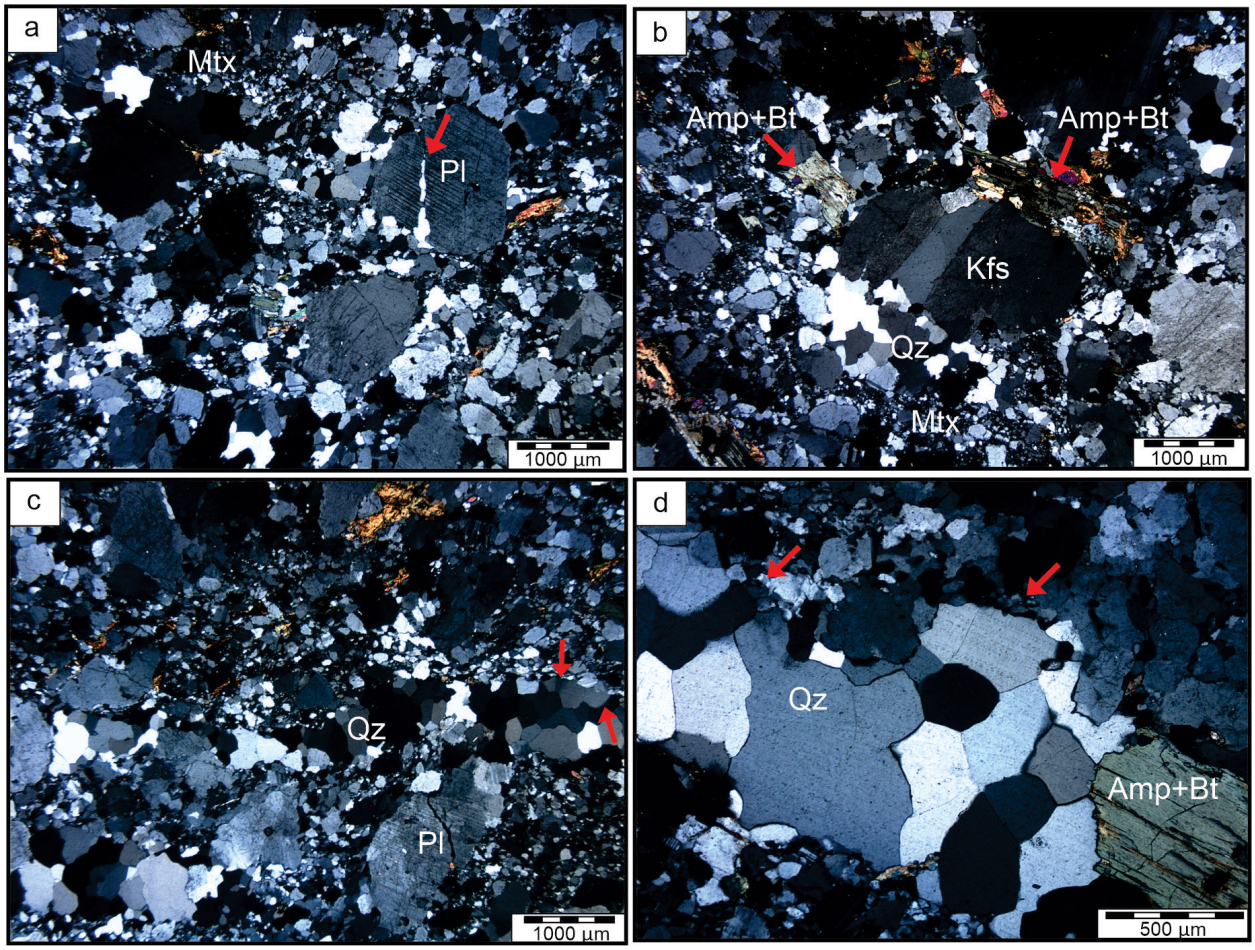

Figure 6. Microstructures of the Catingueira pluton (Qz: quartz; Pl: plagioclase; Kfs: K-feldspar; Amp: amphibole; Bt: biotite; Whitney and Evans 2010; Mtx: fine-grained matrix). (A) Plagioclase porphyroclast exhibiting a microfracture filled with quartz grains (red arrows) and weak deformation twins. (B) K-feldspar clast with undulose extinction wrapped in coarse-grained polycrystalline quartz aggregates and amphibole crystals that are partially altered to biotite (red arrows); (C) Quartz aggregates wrapping around plagioclase porphyroclasts. Subgrain boundaries in quartz grains are indicated by red arrows. (D) Quartz aggregate displaying straight boundaries and polygonal shapes that define triple junctions. Subgrain boundaries are indicated by red arrows. Amphibole occurs as grains parallel to the aggregate elongation.

and in an oblique position (~ 45º) between Z and X (PT247, Fig. 7D), and maxima located at the center of the pole figure in Y (PT249, PT250, GPT2, Figs. 7B, 7C and 7E). The distribution of orientations in samples that have maxima close to Z may define small clusters in intermediate positions in the diagram, such as between Y and Z (PT172), and between Z and X (PT 247).

Misorientation axes (Figs. 8A-8E) for subgrains (2-15º) and for the transition interval between low- and high angle grain boundaries (10-45º) show maxima parallel to the c-axis for all samples, with a limited degree of dispersion of high angle boundaries in samples that have a weaker CPO (e.g. PT172, GPT2, Figs. 8A and 8E).

Correlated misorientation angle distributions (Figs. 8A-8E) show high-frequency of low-angle misorientations for all samples, with peaks between 5 and 10º (Figs. 8A-8E). Uncorrelated distributions deviate from the theoretical random curve in samples that have strong CPO (PT249, PT250); these are accompanied by high frequency peaks of correlated distributions at angles of 40-60º (Fig. 8C).

Mineral chemistry

K-feldspar porphyroclasts of the Santa Terezinha Pluton (Tab. 1) present a variation in Or_{88-96} contents and An values close to zero (Fig. 9A). The high Or values indicate that these feldspars are orthoclase (Fig. 10A). K-feldspar grains from the matrix show Or values ranging from 93 to 94, also classified as orthoclase (Figs. 9A and 10A). The plagioclase has An contents that exhibit little variation (An_{17-20}), with two samples showing lower values (Fig. 9B; $An_{13.3}$ and $An_{15.8}$). Analyses on the rims of fine-grained plagioclase grains from the matrix yield An values of $An_{18.3}$ and $An_{19.8}$, and two analyses on the core of these matrix grains yield values of $An_{18.1}$ and $An_{21.80}$. Most plagioclase samples present little Or content, with one porphyroclast showing $Or_{2.5}$ (Fig. 9B). The plagioclase porphyroclasts and fine grains are classified as oligoclase (Fig. 10A).

The Catingueira pluton shows a compositional variation (Tab. 2) between porphyroclasts and recrystallized matrix of plagioclase samples evidenced mainly by a decrease of An contents in the fine grains (Figs. 9C and 9D). The plagioclase porphyroclasts yield An values of An_{18-20} and the Or content ranges from 0.5 to 2.4 (Fig. 9C). In contrast, plagioclase grains in the matrix are evidenced by a decrease in An content (An_{18-15}) in comparison to the porphyroclasts (0.9; Fig. 9D). The porphyroclasts and recrystallized grains of plagioclase are classified as oligoclase (Fig. 10B). K-feldspar porphyroclasts yield values of Or_{80-100} and are classified as orthoclase (Figs. 9C and 10B).

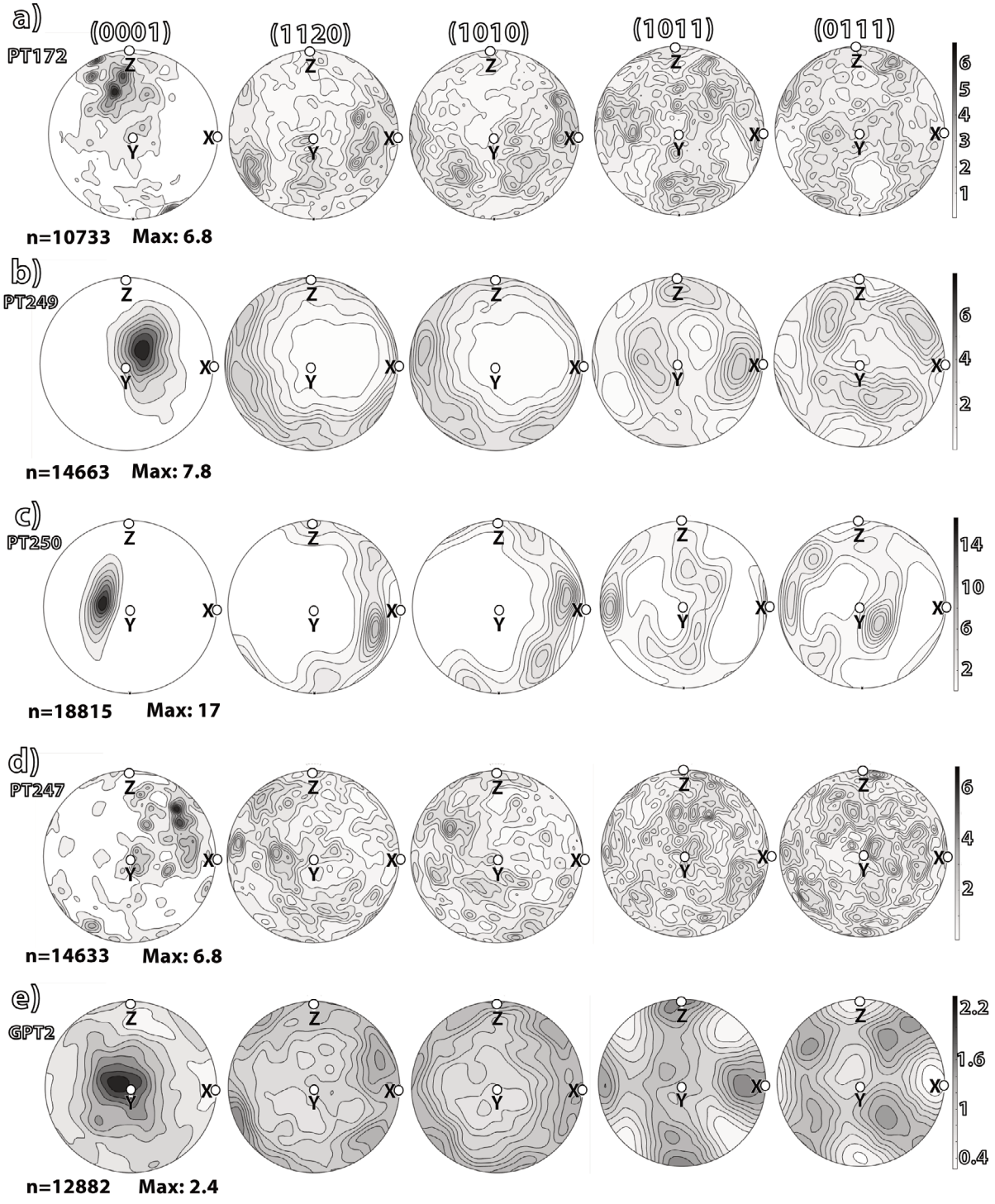

Figure 7. Crystallographic fabrics of quartz grains in the host banded gneisses. See text for discussion.

Zircon U-Pb geochronology

Several samples were collected for geochronological investigation via LA-MC-ICP-MS, but most are poor in zircon. As a result, one sample collected in the SW border of the Santa Terezinha pluton (PUR-02D - 7° 6'16.95"S, 37°25'56.58"W; location in Fig. 1C) is presented here.

The rock is a mylonitic granitoid that crops out at the border of the intrusion, presenting deformed/stretched quartz aggregates in contact with feldspar porphyroclasts (Fig. 5A) as the main microstructural feature. The sample is also poor in zircon and most of the zircon grains are strongly discordant, highly fractured or show strong evidence of metamictization. The small number of recovered zircon crystals show Th/U ratios ranging from 0.38 to 0.63 (Tab. 3). They have an average size of 120 μm, euhedral to subhedral shapes, and axial ratios around 1:3, commonly exhibiting a bipyramidal crystallographic habit (Fig. 11A). The internal structure revealed by backscatter electron (BSE) images shows oscillatory

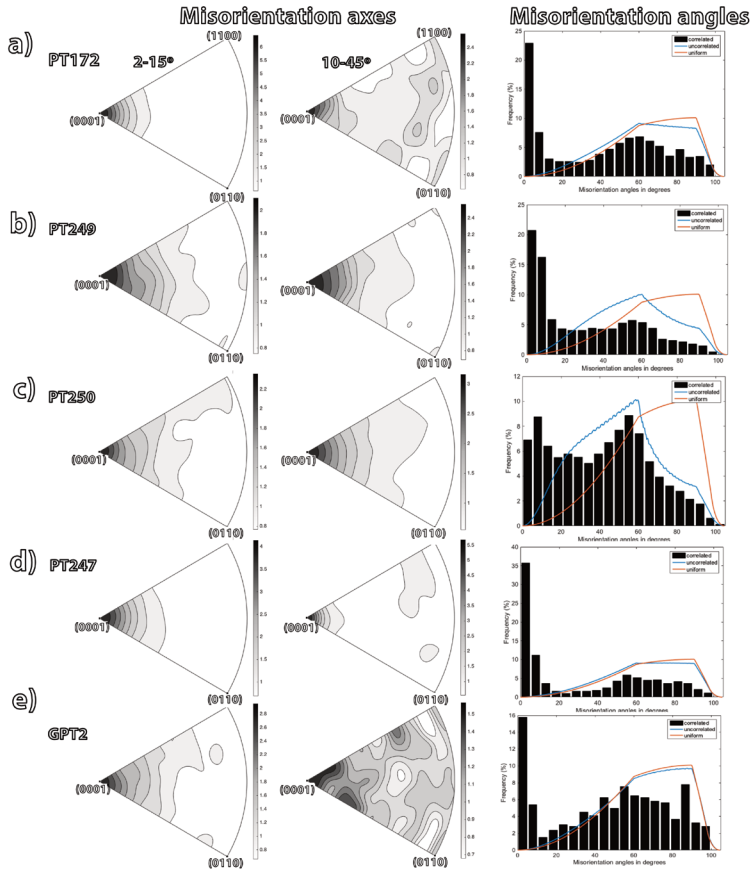

Figure 8. Misorientation axes for low-angle (2-15°) and transitional, low- to high angle (10-45°) boundaries, as well as misorientation angle distributions for the banded gneisses. See text for discussion.

zoning, microfractures with radial to random patterns and a spongy texture, likely due to inner metamictization (Fig. 11A). Small inclusions of unidentified phases are present both in the core and rims of the crystals.

Twenty-nine spots were performed on sample PUR-02D, in which seven concordant spots ranging from 99.58 to 100.92% were plotted in the Concordia diagram (Tab. 3, Fig. 11B). Two of these spots were used to calculate a Concordia age of 625 ± 7 Ma (MSWD = 0.84).

DISCUSSION

Deformation mechanisms in the banded gneisses

Microstructures and EBSD analyses suggest that quartz grains were deformed by dislocation creep (e.g. Hirth and Tullis 1992). The recrystallized quartz grains occur as polycrystalline ribbons around 30 µm, rounded to polygonal shapes, curved to straight boundaries and undulose extinction. The PT172 and PT247 pole figures (Figs. 7A and 7D) show small maxima of the [0001] axis at the periphery of the diagram, close to Z or at intermediate positions (~ 45° from Z along the periphery of the diagram) between Z and X, which suggest dislocation creep along the basal <a> slip system, with a possible minor contribution of slip along rhomb planes (Vauchez 1980, Schmid and Casey 1986, Law 1990). Furthermore, correlated misorientation angle distributions show a high-frequency of low-angle misorientations for all samples, with peaks between 5 and 10° (Figs. 8A-8E).

On the other hand, the observed patterns in PT249, PT250 and GPT2 (Figs. 7B, 7C and 7E) show [0001] maxima located at the center of the pole figure, parallel to Y, supporting that deformation that occurred mainly through dislocation glide along prism planes (Schmid and Casey 1986, Stipp *et al.* 2002, Stipp *et al.* 2004). These samples show uncorrelated distribution of misorientation angles that deviate from the theoretical random curve, a pattern that is accompanied by high-frequency peaks of correlated distributions at angles of 40-60° (Fig. 8C).

The K-feldspar and plagioclase porphyroclasts display intragranular microfractures that crosscut the clasts forming angular fragments (± 800 µm; Fig. 4C), with an offset of up to 50 µm. This observation suggests that the fragments within the fractures are products of the mechanical fragmentation of larger clasts. In addition, the presence of lobate boundaries, core-mantle structures (Fig. 4D), undulose extinction and deformation twins in the clasts point to solid-state strain within the larger porphyroclasts (*e.g.,* Faleiros *et al.* 2010).

All things considered, the current dataset of microstructures and CPO analyses allows us to postulate that mylonitization in the south border of the Patos shear zone was mainly attained via dynamic recrystallization of quartz aggregates and feldspar porphyroclasts. Quartz grains were deformed through subgrain rotation recrystallization with dominant activation of

Table 1. Major representative element chemical analyses for the Santa Terezinha pluton. Table of average of the obtained values.

	PUR-02						
		K-feldspar			Plagioclase		
	Bulk Composition (XRF)	Porphyroclasts	Recrystallized		Porphyroclasts	Recrystallized	
			Core	Rim		Core	Rim
SiO_2	60.08	64.982	62.756	62.523	63.563	63.267	63.616
TiO_2	79.87	0.004	0.013	b.d.l	b.d.l	b.d.l	0.044
Al_2O_3	101.96	19.621	19.697	19.818	22.887	22.423	22.629
FeO	71.84	0.034	0.089	0.114	b.d.l	0.128	0.083
MnO	70.94	0.029	0.012	0.006	0.023	b.d.l	b.d.l
MgO	40.3	b.d.l	b.d.l	b.d.l	b.d.l	b.d.l	0.003
CaO	56.08	b.d.l	b.d.l	b.d.l	4.033	3.999	3.958
Na_2O	61.98	0.532	0.722	0.764	9.057	9.108	9.514
K_2O	94.2	14.64	15.418	15.553	0.247	0.13	0.13
Cr_2O_2	151.99	b.d.l	b.d.l	0.015	0.027	0.036	0.036
NiO	74.69	b.d.l	b.d.l	b.d.l	b.d.l	b.d.l	b.d.l
Total		99.842	98.746	98.792	99.837	99.091	99.977
OH		b.d.l	b.d.l	b.d.l	b.d.l	b.d.l	b.d.l
Si		3.012	2.928	2.913	2.818	2.826	2.809
Ti		b.d.l	0.001	b.d.l	b.d.l	b.d.l	0.001
Al		1.072	1.083	1.088	1.196	1.18	1.177
Cr		b.d.l	b.d.l	0.001	0.001	0.001	b.d.l
Fe		0.001	0.003	0.004	b.d.l	0.005	0.003
Mn		0.001	b.d.l	b.d.l	0.001	b.d.l	b.d.l
Mg		b.d.l	b.d.l	b.d.l	b.d.l	b.d.l	b.d.l
Ca		b.d.l	b.d.l	b.d.l	1.192	0.191	0.187
Na		0.048	0.065	0.069	0.779	0.789	0.814
K		0.866	0.918	0.924	0.014	0.007	0.007
An (%)					19.467	19.379	18.556
Ab (%)		5.234	6.644	6.947	79.113	79.871	80.718
Or (%)		94.766	93.356	93.053	1.42	0.75	0.726

b.d.l.: below detection limit.

the basal and prism dislocation glide system, associated with a local contribution of rhomb planes, whilst feldspars record solid-state recrystallization via core-mantle structures, lobate boundaries and deformation twins in coarse-grained clasts, which can also be affected by localized fracturing (Schmid and Casey 1986, Tullis 2002, Stipp *et al.* 2002, Stipp *et al.* 2004, Fitz Gerald *et al.* 2006, Toy *et al.* 2008, Stipp and Kunze 2008, Stipp *et al.* 2010).

Quartz CPO fabrics defined by the activation of the prism<a> slip system are typical of amphibolite-facies conditions and may record the main peak of deformation conditions of the shear zone (Viegas *et al.* 2014, Archanjo *et al.* 2021). Alternatively, the dominantly basal<a> CPO fabrics may be interpreted as a lower-temperature overprint during the final stages of strain localization and/or subsequent reactivation in the shear zone (*e.g.,* Viegas *et al.* 2014 and references therein). Similarly, late-stage reactivation of previous structures has been systematically documented in other shear zones of the Borborema Province (e.g. Neves *et al.* 2000, Hollanda *et al.* 2010).

Deformation in the Santa Terezinha and Catingueira plutons

The granitic bodies show quartz polycrystalline aggregates with polygonal to irregular shapes, and straight boundaries defining triple junctions (Figs. 5A and 6D). Undulose extinction, subgrains with ca. 50 μm and straight to curved boundaries are also observed. These microstructures suggest that the quartz was recrystallized mainly via a combination of subgrain rotation and grain boundary migration mechanisms (Stipp *et al.* 2002, Passchier and Trouw 2005, Faleiros *et al.* 2010).

The porphyroclasts of K-feldspar and plagioclase have sub-elliptical to rounded shapes and are mainly fractured, producing fragments of intermediate size (± 100 μm) between porphyroclasts and matrix (Figs. 5B, 5C and 5D). Plagioclase and K-feldspar grains in the recrystallized matrix of the Santa Terezinha granite have similar chemical compositions to that of the porphyroclasts (Fig. 9), represented mainly by oligoclase and orthoclase, respectively (Fig. 10). These observations suggest that the smaller fragments were the product of fracturing of the coarse-grained porphyroclasts. In contrast,

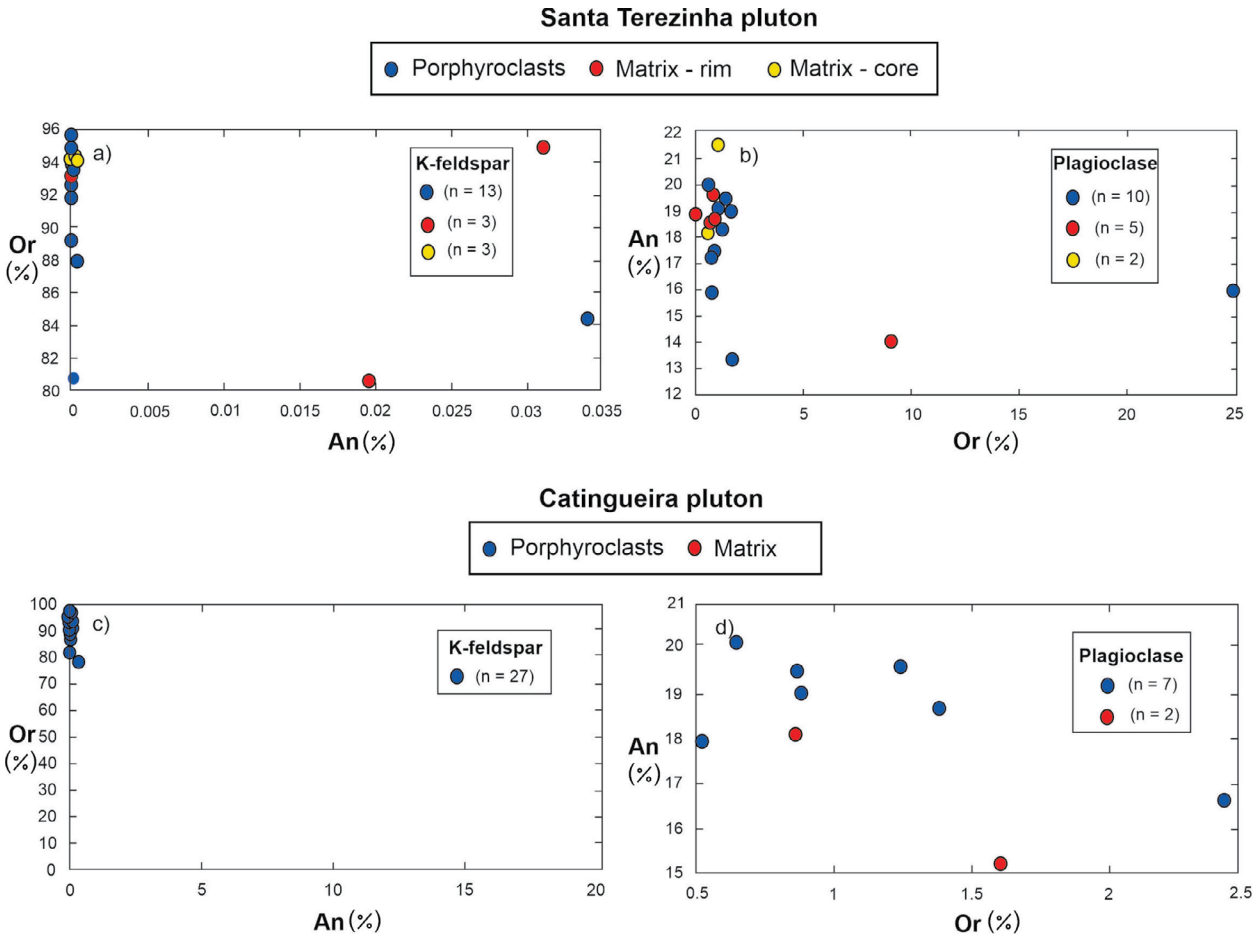

Figure 9. Chemical composition of porphyroclasts and recrystallized grains of K-feldspar and plagioclase in the (A and B) Santa Terezinha and (C and D) Catingueira plutons.

the Catingueira pluton shows differences in the chemical composition of plagioclase porphyroclasts and recrystallized grains (Fig. 9D). Such chemical patterns imply that grain size reduction in feldspar was the result of combined fracturing + nucleation/recrystallization, possibly enhanced by the presence of fluids (Fitz Gerald and Stünitz 1993).

These observations indicate that the microstructure of the plutons results from the activity of dislocation creep as the main deformation/recrystallization mechanism at upper-greenschist/lower-amphibolite facies conditions (Fitz Gerald and Stünitz 1993, Stipp *et al.* 2002, Tullis 2002, Stipp *et al.* 2010).

Granite geochronology in the southern border of the Patos shear zone

Magmatic events in the Patos shear zone have been constrained as being an integral part of the structure's evolution. Evidence for pre-kinematic pluton emplacement was presented by Archanjo *et al.* (2008), who constrained the fabrics and the age behind the emplacement of the Teixeira batholith, which outcrops at the southern boundary of the shear zone. The combined structural data of N-S trending, perpendicular magnetic fabrics and an U-Pb SHRIMP age of 591 ± 5 Ma presented by the authors were interpreted in terms of a pre-kinematic emplacement for the Teixeira batholith, thus suggesting that transcurrent motion in the Patos shear zone is younger than ~ 590 Ma (Archanjo *et al.* 2008).

Synkinematic partial melting in the central portion of the shear zone has been studied by Viegas *et al.* (2014), who analyzed

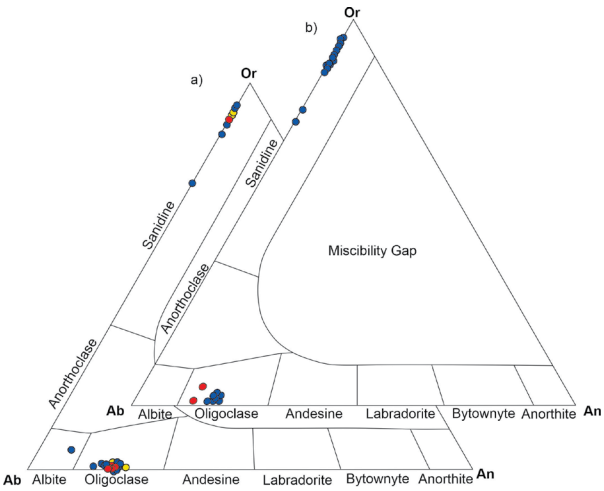

Figure 10. Feldspar classification diagram for the (A) Santa Terezinha pluton and (B) Catingueira pluton.

the overgrowths of zircon grains from diatexites emplaced in the central portion of the shear zone. The obtained U-Pb age of ca. 565 Ma was interpreted by the authors as the peak conditions for the main metamorphic event in the Patos shear zone.

The Santa Terezinha granite shows an elongated shape that is concordant with the main ESE-WNW trend of the Patos shear zone (Fig. 1). This concordant shape suggests that the emplacement of the pluton was synkinematic in relation to the shear zone. The average geochronological result calculated in the Concordia diagram for this pluton provides an early Ediacaran age of 625 ± 7 Ma (Figs. 11A and 11B).

Table 2. Representative chemical analyses for the Catingueira pluton. Table of average obtained values.

	Catingueira pluton				
		K-feldspar		Plagioclase	
	Bulk Composition (XRF)	Porphyroclasts	Recrystallized	Porphyroclasts	Recrystallized
SiO_2	60.08	63.887	63.613	61.514	63.948
TiO_2	79.87	0.004	0.067	b.d.l	b.d.l
Al_2O_3	101.96	19.922	19.703	24.803	22.019
FeO	71.84	0.032	0.01	0.269	0.25
MnO	70.94	0.022	0.026	0.058	0.04
MgO	40.30	b.d.l	0.004	0.014	0.044
CaO	56.08	b.d.l	b.d.l	4.122	3.225
Na_2O	61.98	0.737	0.864	9.292	9.738
K_2O	94.20	15.58	15.437	0.156	0.285
Cr_2O_3	b.d.l	b.d.l	0.012	0.036	b.d.l
Total		100.18	99.73	100.67	99.63
Si		2.94	2.715	2.715	2.832
Ti		1.1	b.d.l	b.d.l	b.d.l
Al		b.d.l	1.29	1.29	1.149
Cr		b.d.l	0.002	0.002	b.d.l
Fe		0.001	0.001	0.001	0.009
Mn		0.001	b.d.l	b.d.l	0.002
Mg		b.d.l	b.d.l	b.d.l	0.003
Ca		b.d.l	1.192	1.192	0.153
Na		0.066	0.786	0.786	0.836
K		0.914	0.012	0.012	0.016
An (%)		0	19.377	19.377	15.222
Ab (%)		6.707	79.372	79.372	83.176
Or (%)		93.293	1.25	1.25	1.602

b.d.l.: below detection limit.

Table 3. LA-MC-ICP-MS U-Pb data used for U-Pb age calculation in the Santa Terezinha pluton.

	Isotopic ratios					
Grain spot	207Pb/206Pb	± (2σ)	207Pb/235U	± (2σ)	206Pb/238U	± (2σ)
PUR-02D-05	0.07	2.32	1.33	2.41	0.14	0.65
PUR-02D-12	0.07	3.13	1.91	3.89	0.18	2.31
PUR-02D-13	0.07	2.14	2.29	2.35	0.14	0.1
PUR-02D-27	0.06	2.21	0.84	2.6	0.1	1.36
PUR-02D-33	0.06	2.25	0.85	3.05	0.1	2.05
PUR-02D-39	0.06	2.26	0.91	2.8	0.11	1.63
PUR-02D-41	0.06	2.95	1.03	3.25	0.12	1.38

	Ages								
Grain spot	207Pb/206Pb	± (2σ)	207Pb/235U	± (2σ)	206Pb/238U	± (2σ)	Rho	Th/U	Conc. (%)
PUR-02D-05	845	48	860	14	866	5	0.27	0.38	100.79
PUR-02D-12	1,074	60	1,082	25	1,087	23	0.54	0.63	100.43
PUR-02D-13	832	44	844	13	850	8	0.42	0.43	100.74
PUR-02D-27	598	47	620	12	626	8	0.52	0.42	100.92
PUR-02D-33	617	49	624	14	625	12	0.67	0.46	100.18
PUR-02D-39	660	49	656	13	656	10	0.58	0.51	99.85
PUR-02D-41	722	63	719	17	716	9	0.42	0.42	99.58

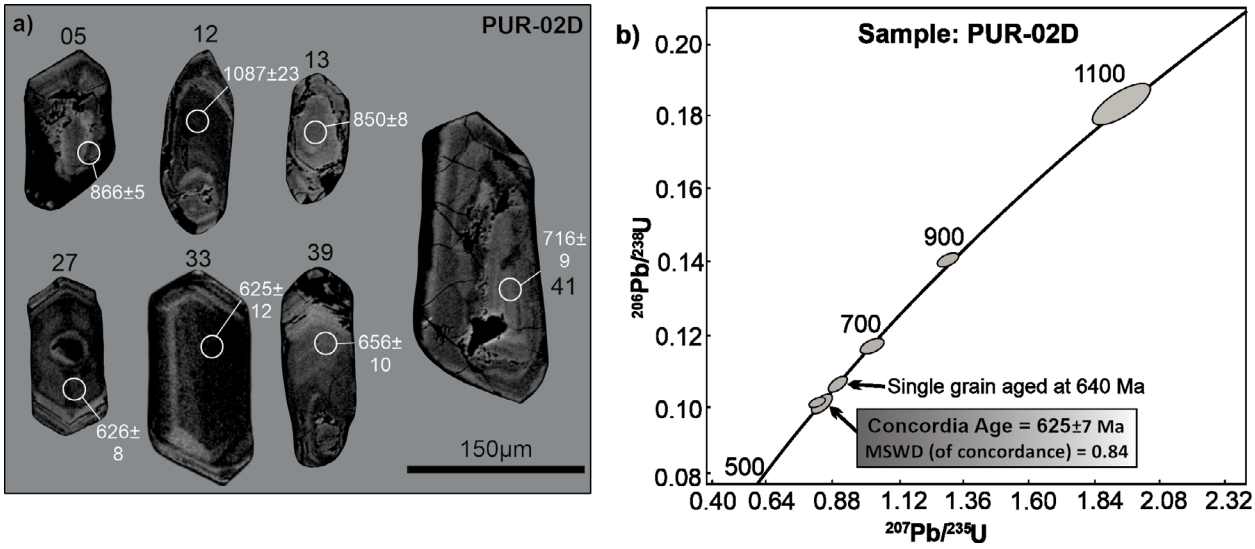

Figure 11. (A) Backscatter electron images of zircon grains from sample PUR-02D. (B) Concordia plot for the PUR-02D zircon spots with a lower 5% discordance displaying the main age of 625 ± 7 Ma.

Two possibilities can be considered in order to reconcile the apparent contrast between the field, microstructural and geochronological data of the Santa Terezinha granitoid: the pluton is pre-kinematic in comparison to the Patos shear zone, being emplaced at ~ 625 Ma and subsequently elongated and stretched along the main shear trend. This would result in the pluton shape and its mylonitic structure; the pluton is synkinematic in comparison to the Patos shear zone, but the obtained zircon age of ~ 625 Ma represents inheritance from host rocks or even previous hidden magmatic pulses.

Ancient, unexpected ages related to *en-cornue* intrusions have been recently documented along other shear zones of the Borborema Province (Weinberg *et al.* 2004, Santos *et al.* 2020). Furthermore, recent thermochronological investigations based on the closure temperatures of hornblende and biotite analyzed via $^{40}Ar/^{39}Ar$ dating have constrained slow- to moderate cooling rates of ~ 17º C/Ma in the central sector of the Patos shear zone (Archanjo *et al.* 2021). Such evidence would suggest that the timing between magma emplacement and strike-slip deformation in the shear zones of the Borborema Province might have been protracted.

At last, it's important to note some key evidence gathered in this study, composed of: the elongated shape of the pluton, concordant with the shear zone orientation and its mylonitized texture, which results from deformation at the boundaries of the shear zone, and the present age of ~ 625 Ma, allow us to speculate that this intrusion is pre-kinematic in comparison to the Patos shear zone. Given its relatively small dimensions, it may have been elongated and stretched along the trend of the shear zone during and/or after its peak metamorphic event, currently dated at ~ 565 Ma (Viegas *et al.* 2014). Post-emplacement, shape adjustment of early (≥ 590 Ma) granitoid intrusions has been documented in plutons that are mainly located at the southern boundary of the Patos shear zone (Archanjo and Fetter 2004, Archanjo *et al.* 2008), and a process similar to these mechanisms may have affected the Santa Terezinha granitoid.

Though the current evidence presented in this study does not allow us to fully discard a hypothesis of an inherited age from the source, field and microstructural evidence suggest that shearing associated with the Patos shear zone may have modified the pluton from its original form to its current, elongated shape. As of yet, more geochronological and structural data on this granite — and associated intrusions, e.g., the Catingueira pluton — are necessary in order to better constrain the chronology of the magmatism and deformation in this complex sector of the Borborema Province.

CONCLUSIONS

Based on meso- and microscale structures, bulk rock and mineral chemistry as well as U-Pb geochronology, the following conclusions can be drawn from this study:

- The microstructures and CPO analysis of the banded gneisses point to the dominance of solid-state, medium- to high-grade deformation mechanisms in the south border of the Patos shear zone. Quartz is mainly recrystallized via subgrain rotation, while feldspar deforms via the development of core-mantle structures and localized fracturing;
- Quartz crystallographic fabrics reveal the dislocation glide mainly along the basal and prism planes, with minor contributions of rhomb slip. CPO fabrics evidenced by the activity of prism<a> slip are developed during shearing at high-temperatures, while the CPOs that record dominance of basal slip are attributed to a subsequent overprint and/or reactivation event in the Patos shear zone;
- The Santa Terezinha and Catingueira plutons show recrystallization accommodated mainly by dislocation creep at upper greenschist/lower amphibolite facies conditions (~ 500°C), similar to the host banded gneisses. The microstructures reveal that quartz was recrystallized through a combination of subgrain rotation and grain boundary migration, while the feldspars mostly record brittle fragmentation and the subsequent formation of heterogeneously sized fragments;

- The Santa Terezinha pluton presents an early Ediacaran age of 625 ± 7 Ma, which is considered the best estimate for magmatic crystallization of the pluton;
- The combination of geochronological and structural data suggests that the Santa Terezinha granite was emplaced before the main peak metamorphic conditions recorded in the Patos shear zone, currently dated at ~ 565 Ma. Ductile shearing led to elongation and stretching of the plutonic body to a concordant shape along the shear zone trend. Post-emplacement, shape modification of granitoid intrusions has been documented in shear zones from the Borborema Province and a similar process may have affected the Santa Terezinha (and possibly the Catingueira) pluton.

ACKNOWLEDGEMENTS

This research was funded by CAPES (grant nº 88882.383270/2019-01), Fundação de Apoio à Pesquisa do Distrito Federal (FAPDF, grant nº 0193.001510/2017) and Fundação de Amparo à Pesquisa do Estado de São Paulo (FAPESP, grant nº 09/17537-1). LCMLS is thankful for the support given by the Instituto Nacional de Ciência e Tecnologia de Estudos Tectônicos — CNPq. We are indebted to the very detailed and pertinent reviews of Sérgio P. Neves and an anonymous reviewer, which greatly improved the manuscript. We thank Dr. Roberto Ventura Santos and Dr. Guilherme Gonçalves for help in the acquisition of geochronological data. The staff at *Géosciences Montpellier* is thanked for their assistance during EBSD analysis. We thank Paulo Castellan for his participation and help during fieldwork.

ARTICLE INFORMATION

Manuscript ID: 20210048. Received on: 06/25/2021. Approved on: 10/03/2021

C.S. conducted fieldwork, performed petrographic and microstructural analyses, developed analytical work on the collected samples, treated the obtained geochronological data and wrote the original draft of the manuscript. L.V. conducted fieldwork, supervised the microstructural and mineral chemistry analyses, reviewed/edited the original draft of the manuscript and acquired funding for the development of this research. L.S.treated the obtained geochronological data and reviewed/edited the original draft of the manuscript.

Competing interests: The authors declare no competing interests.

REFERENCES

Almeida F.F.M. 1967. Origem e evolução da plataforma brasileira. *Boletim DNPM/DGM*, **241**. 36 p.

Almeida F.F.M., Hasui Y., Brito Neves B.B., Fuck R.A. 1981. Brazilian structural provinces: an introduction. *Earth Science Reviews*, **17**(1-2):1-29. https://doi.org/10.1016/0012-8252(81)90003-9

Archanjo C.J., Fetter A.H. 2004. Emplacemente setting of the granite sheeted pluton of Esperança (Brasiliano orogen, Northeastern Brazil). *Precambrian Research*, **135**(3):193-215. http://doi.org/10.1016/j.precamres.2004.08.008

Archanjo C.J., Hollanda M.H.B.M., Rodrigues S.W.O., Brito Neves B.B., Armstrong R. 2008. Fabrics of pre- and syntectonic granite plutons and chronology of shearzones in the Eastern Borborema, NE Brazil. *Journal of Structural Geology*, **30**(3):310-326. https://doi.org/10.1016/j.jsg.2007.11.011

Archanjo C.J., Hollanda M.H.B.M., Viegas L.G.F. 2021. Late Ediacaran lateral-escape tectonics as recorded by the Patos shear zone (Borborema Province, NE Brazil). *Brazilian Journal of Geology*, **51**(2):e20200132. https://doi.org/10.1590/2317-4889202120200132

Archanjo C.J., Trindade R.I.F., Bouchez J.L., Ernesto M. 2002. Granite fabrics andregional-scale strain partitioning in the Seridó belt (Borborema Province, NEBrazil). *Tectonics*,**21**(1):3-1-3-14.http://dx.doi.org/10.1029/2000TC001269

Archanjo C.J., Viegas L.G., Hollanda M.H.B.M., Souza L.C., Liu D. 2013. Timing of the HT/LP transpression in the Neoproterozoic Seridó Belt (Borborema Province, Brazil): constraints from U–Pb (SHRIMP) geochronology and implications forthe connections between NE Brazil and West Africa. *Gondwana Research*, **23**(2):701-714. http://dx.doi.org/10.1016/j.gr.2012.05.005

Brito Neves B.B., Passarelli C.R., Basei M.A.S., Santos E.J. 2003. Idades U-Pb em zircão de alguns granitos clássicos da Província Borborema. *Geologia USP. Série Científica*, **3**:25-38. https://doi.org/10.5327/S1519-874X2003000100003

Brito Neves B.B., Santos E.J., Van Schmus W.R. 2000. Tectonic history of the Borborema province. *In*: Cordani U.G., Milani E.J., Thomaz Filho A., Campos D.A. (Eds.). *Tectonic Evolution of South América*. Rio de Janeiro, 31st International Geological Congress, p. 151-182.

Brown M., Solar G.S. 1998. Granite ascent and emplacement during contractional deformation in convergent orogens. *Journal of Structural Geology*, **20**(9-10):1365-1393. https://doi.org/10.1016/S0191-8141(98)00074-1

Brown M., Solar G.S. 1999. The mechanism of ascent and emplacement of granite magma during transpression: a syntectonic granite paradigm. *Tectonophysics*, **312**(1):1-33. http://doi.org/10.1016/s0040-1951(99)00169-9

Caxito F.A., Santos L.C.M.L., Ganade C.E., Bendaoud A., Fettous E., Bouyo M.H. 2020. Toward an integrated model of geological Evolution for NE Brazil-NW Africa: the Borborema Province and its connections to the Trans-Saharan (Benino-Nigerian and Tuareg shields) and Central African orogens. *Brazilian Journal of Geology*, **50**(2):e20190122. https://doi.org/10.1590/2317-4889202020190122

Corsini M., Vauchez A., Archanjo C.J., Jardim de Sá E.F. 1991. Strain transfer at a continental scale from a transcurrent shear zone to a transpressional fold belt: the Patos-Seridó belt system, north-eastern Brazil. *Geology*, **19**(6):586-589. https://doi.org/10.1130/0091-7613(1991)019%3C0586:STACSF%3E2.3.CO;2

Faleiros F.M., Campanha G.A.C., Bello R.M.S., Fuzikawa K. 2010. Quartz recrystallizations regimes, c-axis texture transition and fluid inclusion reequilibration in a prograde greenschist to amphibolite facies mylonite zone (Ribeira Shear Zone, SE Brazil). *Tectonophysics*, **485**(1-4):193-214. https://doi.org/10.1016/j.tecto.2009.12.014

Fitz Gerald J.D., Mancktelow N.S., Pennacchioni G., Kunze K. 2006. Ultrafine-grained quartz mylonites from high-grade shear zones: Evidence for strong dry middle to lower crust. *Geology*, **34**(5):369-372. https://doi.org/10.1130/G22099.1

Fitz Gerald J.D., Stünitz H. 1993. Deformation of granitoids at low metamorphic grade. I: Reactions and grain size reduction. *Tectonophysics*, **221**(3-4):269-297. https://doi.org/10.1016/0040-1951(93)90163-E

Guimarães I.P., Silva Filho A.F., Almeida C.N., Van Schmus W.R., Araújo J.M.M., Melo S.C., Melo E.B. 2004. Brasiliano (Pan-African) granitic magmatism in the Pajeú-Paraíba belt, Northeast Brazil: an isotopic and geochronological approach. *Precambrian Research*, **135**(1-2):23-53. https://doi.org/10.1016/j.precamres.2004.07.004

Hielscher R., Schaeben H. 2008. A novel pole figure inversion method: Specification of the MTEX algorithm. *Journal of Applied Crystallography*, **41**(6):1024-1037. https://doi.org/10.1107/S0021889808030112sche

Hirth G., Tullis J. 1992. Dislocation creep regimes in quartz aggregates. *Journal of Structural Geology*, **14**(2):145-159. https://doi.org/10.1016/0191-8141(92)90053-Y

Hollanda M.H.B.M., Archanjo C.J., Souza L.C., Armstrong R., Vasconcelos P.M. 2010. Cambrian mafic to felsic magmatism and its connections with transcurrent shear zones of the Borborema Province (NE Brazil): Implications for the late assembly of the West Gondwana. *Precambrian Research*, **178**(1-4):1-14. https://doi.org/10.1016/j.precamres.2009.12.004

Horstwood M.S.A., Košler J., Gehrels G., Jackson S.E., McLean N.M., Paton C., Pearson N.L., Sircombe K., Sylvester P., Vermeesch P., Bowring J.F., Condon D.J., Schoene B. 2016. Community-derived standards for LA-ICP-MS U-(Th-)Pb geochronology - uncertainty propagation, age interpretation and data reporting. *Geostandards and Geoanalytical Research*, **40**(3):311-332. https://doi.org/10.1111/j.1751-908X.2016.00379.x

Hutton D.H.W. 1988. Granite emplacement mechanisms and the tectonic controls: inferences from deformation studies. *Transactions of the Royal Society of Edinburgh: Earth Sciences*, **79**(2-3):245-255. https://doi.org/10.1017/S0263593300014255

Jackson S.E., Pearson N.J., Griffin W.L., Belousova E.A. 2004. The application of laser ablation-inductively coupled plasma-mass spectrometry to in situ U–Pb zircon geochronology. *Chemical Geology*, **211**(1-2):47-69. https://doi.org/10.1016/j.chemgeo.2004.06.017

Law R.D. 1990. Crystallographic fabrics: a selective review of their applications to research in structural geology. *In*: Knipe R., Rutter E. (Eds.). *Deformation mechanisms, rheology and tectonics*. Geological Society of London, Special Publication, 54. p. 335-352.

Ludwig K.R. 1993. *New Isoplot Version 2.2*. Berkeley: Berkeley Geochronology Center.

Neves S.P., Mariano G., Barros Correia P., Silva J.M.R. 2006. 70 m.y. of synorogenic plutonism in eastern Borborema Province (NE Brazil): temporal and kinematic constraints on the Brasiliano Orogeny. *Geodinamica Acta*, **19**(3-4):213-236. https://doi.org/10.3166/ga.19.213-236

Neves S.P., Vauchez A., Feraud G. 2000. Tectono-thermal evolution, magma emplacement, and shear zone development in the Caruaru area (Borborema Province, NE Brazil). *Precambrian Research*, **99**(1-2):1-32. https://doi.org/10.1016/S0301-9268(99)00026-1

Passchier C.W., Trouw R.A.J. 2005. *Microtectonics*. 2. ed. Berlin: Springer.

Paterson S.R., Fowler Jr. T.K., Schmidt K.L., Yoshinobu A.S., Yuan E.S., Miller R.B. 1998. Interpreting magmatic fabric patterns in plutons. *Lithos*, **44**(1-2):53-82. https://doi.org/10.1016/S0024-4937(98)00022-X

Paterson S.R., Tobisch O.T. 1992. Rates of geological processes in magmatic arcs: implications for the timing and nature of pluton emplacement and wall-rock deformation. *Journal of Structural Geology*, **14**(3):291-300. https://doi.org/10.1016/0191-8141(92)90087-D

Paton C., Hellstrom J., Paul B., Woodhead J., Hergt J. 2011. Iolite: Freeware for the visualisation and processing of mass spectrometric data. *Journal of Analytical Atomic Spectrometry*, **26**(12):2508-2518. https://doi.org/10.1039/C1JA10172B

Petrus J.A., Kamber B.S. 2012. VizualAge: A novel approach to laser ablation ICP-MS U-Pb geochronology data reduction. *Geostandards and Geoanalytical Research*, **36**(3):247-270. https://doi.org/10.1111/j.1751-908X.2012.00158.x

Rosenberg C.L. 2004. Shear zones and magma ascent: a model based on a review of the Tertiary magmatism in the Alps. *Tectonics*, **23**(3):TC3002. https://doi.org/10.1029/2003TC001526

Santos E.J., Medeiros V.C. 1999. Constraints from granitic plutonism on Proterozoic crustal growth of the Transverse Zone, Borborema Province, NE Brazil. *Revista Brasileira de Geociências*, **29**(1):73-84. http://dx.doi.org/10.25249/0375-7536.1999297384

Santos L.C.M.L., Lima H.M., Lages G.A., Caxito F.A., Araújo Neto J.F., Guimarães I.P. 2020. Petrogenesis of the Riacho do Icó Stock: Evidence for Neoproterozoic slab melting during accretion tectonics in the Borborema Province? *Brazilian Journal of Geology*, 50(2):e20190127. https://doi.org/10.1590/2317-4889202020190127

Santos L.C.M.L., Oliveira R.G., Lages G.A., Dantas E.L., Caxito F.A., Cawood P.A., Fuck R.A., Lima H.M., Santos G.L., Araújo Neto J.F. 2021. Evidence for Neoproterozoic terrane accretion in the central Borborema Province, West Gondwana deduced by isotopic and geophysical data compilation. *International Geology Review*. https://doi.org/10.1080/00206814.2021.1944332

Santos L.C.M.L., Viegas L.G., 2021. Exploring the relationships between shear zones and granites: field and microstructural data for contrasting case studies of the Borborema Province (NE Brazil). *Geologia USP. Série Científica*, **21**(2):3-18. https://doi.org/10.11606/issn.2316-9095.v21-180579

Schmid S.M., Casey M. 1986. Complete fabric analysis of some commonly observed quartz [c]-axis patterns. *In*: Hobbs B.E., Heard H.C. (Eds.), *Mineral and Rock Deformation: Laboratory Studies*, **36**. American Geophysical Union, Geo-physical Monograph, p. 263-286.

Schmidt K.L., Paterson S.R. 2000. Analyses fail to find coupling between deformation and magmatism. *Eos, Transactions American Geophysical Union*, **81**(18):197-203. https://doi.org/10.1029/00EO00133

Sial A.N. 1986. Granite-types in northeast Brazil: current knowledge. *Revista Brasileira de Geociências*, **16**(1):54-72.

Sial A.N., Ferreira V.P. 2016. Magma associations in Ediacaran granitoids of the Cachoeirinha-Salgueiro and Alto Pajeú terranes, northeastern Brazil: forty years of studies. *Journal of South American Earth Sciences*, **68**, 113-133. https://doi.org/10.1016/j.jsames.2015.10.005

Stipp M., Fügenschuh B., Gromet L.P., Stünitz H., Schmid S.M. 2004. Contemporaneous plutonism and strike-slip faulting: a case study from the Tonale fault zone north of the Adamello pluton (Italian Alps). *Tectonics*, **23**(3):TC3004. https://doi.org/10.1029/2003TC001515

Stipp M., Kunze K. 2008. Dynamic recrystallization near the brittle-plastic transition in naturally and experimentally deformed quartz aggregates. *Tectonophysics*, **448**(1-4):77-97. https://doi.org/10.1016/j.tecto.2007.11.041

Stipp M., Stünitz H., Heilbronner R., Schmid S.M. 2002. The eastern Tonale fault zone: a 'natural laboratory' for crystal plastic deformation of quartz over a temperature range from 250 to 700°C. *Journal of Structural Geology*, **24**(12):1861-1884. https://doi.org/10.1016/S0191-8141(02)00035-4

Stipp M., Tullis J., Scherwath M., Behrmann J.H. 2010. A new perspective on paleopiezometry: Dynamically recrystallized grain size distributions indicate mechanism changes. *Geology*, **38**(8):759-762. https://doi.org/10.1130/G31162.1

Toy V.G., Prior D.J., Norris R.J. 2008. Quartz fabrics in the Alpine Fault mylonites: Influence of pre-existing preferred orientations on fabric development during progressive uplift. *Journal of Structural Geology*, **30**(5):602-621. https://doi.org/10.1016/j.jsg.2008.01.001

Tullis J. 2002. Deformation of granitic rocks: Experimental studies and natural examples. *Reviews in Mineralogy and Geochemistry*, **51**(1):51-95. https://doi.org/10.2138/gsrmg.51.1.51

Van Schmus W.R., Brito Neves B.B., Hackspacher P., Babinski M. 1995. U/Pb and Sm/Nd geochronolgic studies of eastern Borborema Province, northeastern Brazil: initial conclusions. *Journal of South American Earth Sciences*,**8**(3-4):267-288.https://doi.org/10.1016/0895-9811(95)00013-6

Van Schmus W.R., Kozuch M., Brito Neves B.B. 2011. Precambrian history of the Zona Transversal of the Borborema Province, NE Brazil: Insights from Sm-Nd and U-Pb geochronology. *Journal of South American Earth Sciences*, **31**(2-3):227-252. https://doi.org/10.1016/j.jsames.2011.02.010

Van Schmus W.R., Oliveira E.P., Silva Filho A.F., Toteu S.F., Penaye J., Guimarães I.P. 2008. Proterozoic links between the Borborema Province, NE Brazil, and the Central African Fold Belt. *In*: Pankhurst R.J., Trouw R.A.J., Brito Neves B.B., DeWit M.J. (Eds.). *West Gondwama:* Pre-Cenozoic Correlations Across the South Atlantic Region, v. 294. Geological Society of London, Special Publications, p. 69-99. http://dx.doi.org/10.1144/SP294.5

Vauchez A. 1980. Ribbon texture and deformation mechanisms of quartz in a mylonitized granite of Great Kabylia (Algeria). *Tectonophysics*, **67**(1-2):1-12. https://doi.org/10.1016/0040-1951(80)90160-2

Vauchez A., Neves S., Caby R., Corsini M., Egydio-Silva M., Arthaud M., Amaro V. 1995. The Borborema shear zone system, NE Brazil. *Journal of South American Earth Sciences*, **8**(3-4):247-266. https://doi.org/10.1016/0895-9811(95)00012-5

Vauchez A., Tommasi A., Neves S.P. 1997. Transcurrent shear zones and magma emplacement in Neoproterozoic belts of Brazil. *In*: Bouchez J.L., Hutton D.H.W., Stephens W.E. (eds.), *Granite:* from segregation of melt to emplacement fabrics. Boston: Kluwer, p. 275-293.

Viegas L.G.F., Archanjo C.J., Hollanda M.H.B.M., Vauchez A. 2014. Microfabrics and zircon U–Pb (SHRIMP) chronology of mylonites from the Patos shear zone (Borborema Province, NE Brazil). Precambrian Research, **243**:1-17. https://doi.org/10.1016/j.precamres.2013.12.020

Vigneresse J.L. 1995. Control of granite emplacement by regional deformation. *Tectonophysics*,**249**(3-4):173-186.https://doi.org/10.1016/0040-1951(95)00004-7

Weinberg R.F., Sial A.N., Mariano G. 2004. Close spatial relationship between plutons and shear zones. *Geology*, **32**(5):377-380. https://doi.org/10.1130/G20290.1

Whitney D.L., Evans B.W. 2010. Abbreviations for names of rock-forming minerals. *American Mineralogist*, **95**(1):185-187. https://doi.org/10.2138/am.2010.3371

Wiedenbeck M., Allé P., Corfu F., Griffin W.L., Meier M., Oberli F., Von Quadt A., Roddick J.C., Spiegel W. 1995. Three Natural Zircon Standards for U-Th-Pb, Lu-Hf, Trace Element and REE Analyses. *Geostandards and Geoanalytical Research*, **19**(1):1-23. https://doi.org/10.1111/j.1751-908X.1995.tb00147.x